JACS
JOURNAL OF THE AMERICAN CHEMICAL SOCIETY

Communication

pubs.acs.org/JACS

Pore-Engineered Metal–Organic Frameworks with Excellent Adsorption of Water and Fluorocarbon Refrigerant for Cooling Applications

Jian Zheng,[†] Rama S. Vemuri,[‡] Luis Estevez,[‡] Phillip K. Koech,[‡] Tamas Varga,[§] Donald M. Camaioni,[†] Thomas A. Blake,[†] B. Peter McGrail,[‡] and Radha Kishan Motkuri*[,‡]

[†]Physical and Computational Sciences Directorate, Pacific Northwest National Laboratory, Richland, Washington 99354, United States

[‡]Energy and Environment Directorate, Pacific Northwest National Laboratory, Richland, Washington 99354, United States

[§]Environmental Molecular Sciences Laboratory, Pacific Northwest National Laboratory, Richland, Washington 99354, United States

Supporting Information

ABSTRACT: Metal–organic frameworks (MOFs) have shown promising behavior for adsorption cooling applications. Using organic ligands with 1, 2, and 3 phenylene rings, we construct moisture-stable Ni-MOF-74 members with adjustable pore apertures, which exhibit excellent sorption capabilities toward water and fluorocarbon R134a. To our knowledge, this is the first report of adsorption isotherms of fluorocarbon R134a in MOFs. The adsorption patterns for these materials differ significantly and are attributed to variances in their hydrophobic/hydrophilic pore character associated with differences in pore size.

The sorption of vapor on the surface of a solid is accompanied by heat generation and consumption. Such processes have been widely used in cooling applications for decades.[1] According to the U.S. Department of Energy, more than 40% of all energy consumption in American homes is a result of cooling and heating.[2] Moreover, conventional cooling/heating systems generate increased CO_2 emissions. Thus, sorption-based, eco-friendly, highly efficient adsorption cooling systems have gained greater attention recently.[3]

The efficiency of adsorption cooling systems depends on the adsorbate–adsorbent working pairs. Traditionally, porous materials such as silica gels, activated carbons, and zeolites were examined as adsorbents. However, they suffer from lack of tunability and functionalization. Lately, highly modular metal–organic frameworks (MOFs) have been designed to provide thermal and chemical stability, high surface area, and large pore volumes.[4] These MOFs provide targeted adsorption behavior and enhanced loading capacities for applications like novel adsorption chiller systems.[5]

Because most MOFs are hydrophilic in nature, their use in water sorption-based adsorption cooling applications is of interest.[6,7] Water is a preferred adsorbate owing to its abundance, harmlessness, and high evaporation enthalpy.[8] However, because of its low saturation pressure, the diffusion rate of water is seriously limited, and its use in an adsorption cooling application requires the system to be strictly vacuum-tight.[9] Additionally, water cannot be used in cases requiring an operating temperature below 0 °C. Conversely, hydrofluorocarbon refrigerants can be operated above atmospheric pressures because their chemical stability yields an adsorbate with suitable saturated vapor pressures and boiling points, which makes them attractive despite their lower latent heats of vaporization.[10] Among the various fluorocarbon refrigerants, R134a (CH_2FCF_3, 1,1,1,2-tetrafluoroethane) is promising for cooling applications due to its low boiling temperature and zero ozone depletion potential. In our recent work, we found that fluorocarbon refrigerants exhibited exceptionally high uptake and reversible adsorption properties in porous MOFs.[3] Therefore, MOFs/fluorocarbon working pairs can be exploited for eco-friendly adsorption cooling applications given that higher gas uptake is indicative of higher working capacity for such practical applications.

Understanding the effects of pore structure and framework topology on the adsorption of guest molecules in pores is crucial for designing MOFs. Although previous studies have shown that the pore environment plays a crucial role in MOF applicability for gas storage,[11] separation,[12] water treatment,[13] and catalysis,[14] less significant effort has been devoted to investigating the influence of pore environment on the adsorption properties of either water or fluorocarbon in MOFs.[8,9,15,16] Herein we report the effects of pore engineering MOF-74 on sorption properties of water and fluorocarbon refrigerants. MOF-74 has been extensively studied mainly due to the open metal sites as well as 1D cylindrical pores, which show interesting gas adsorption and separation properties.[17,18] The Yaghi group has introduced the pore-engineering concept in Mg-MOF-74 frameworks by using original linkers with 2 to 11 phenylene units to construct the Mg-MOF-74 frameworks with increased pore apertures from 14 to 98 Å.[19,20] However, DeCoste et al. observed the morphological instability of Mg-MOF-74 after exposure to water vapor.[21] Given its relatively good stability in humid environments,[22] we applied this pore engineering concept to the more robust Ni-MOF-74 structure by changing the length of the organic linker using a previously reported methodology.[19] We then investigated the effect of

Received: May 11, 2017
Published: July 13, 2017

DOI: 10.1021/jacs.7b04872
J. Am. Chem. Soc. 2017, 139, 10601–10604

pore environment on the adsorption of water and R134a for potential use in adsorption cooling applications.

We synthesized three Ni-MOF-74 analogues, namely Ni-MOF-74, Ni-MOF-74-BPP (BPP = 3,3′-dioxido-4,4′-biphenyldicarboxylate, biphenyl with *para*-COOH) (hereafter Ni-BPP), and Ni-MOF-74-TPP (TPP = 3,3′-dioxido-4,4′-triphenyldicarboxylate, triphenyl with *para*-COOH) (hereafter Ni-TPP). As shown in Figures 1, S7, and S8, the structure consists of

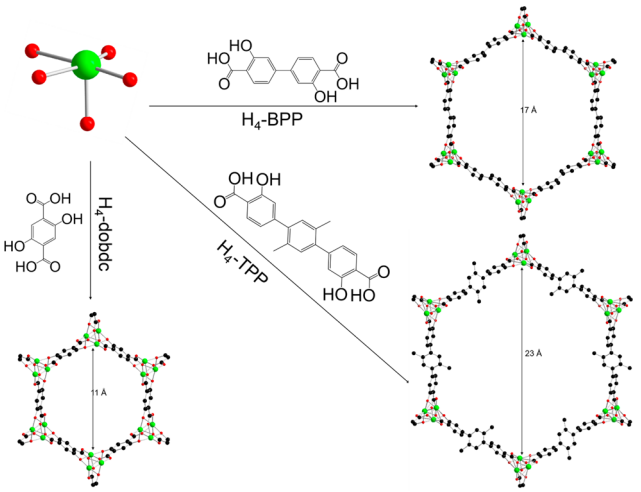

Figure 1. Schematic representation of the Ni^{2+} node, organic bridging ligands, and the corresponding structures (as viewed along the *c*-axis) of the pore-expanded Ni-MOF-74 analogues. Green, red, and black spheres represent Ni, O, and C atoms, respectively. For simplicity, H atoms not shown.

inorganic Ni^{2+} nodes coordinated to ligands with 1, 2, and 3 phenylene rings to form 3D hexagonal channels. We further confirmed these cylindrical pores via TEM (Figure 2). The crystal structures of synthesized samples were analyzed using powder X-ray diffraction (PXRD) and Rietveld refinements. There is good agreement between PXRD patterns and models. 100% phase purity was assumed because no secondary phase peaks were observed in diffraction patterns (Figures 2a, S9, and

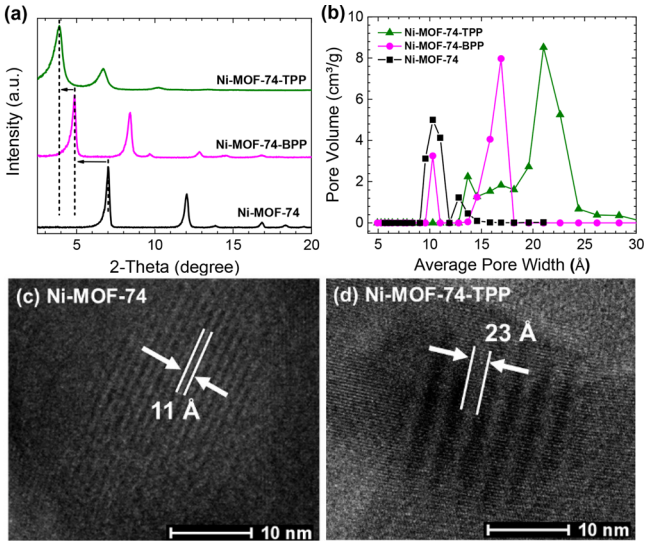

Figure 2. XRD patterns (a) and pore size distributions (b) of pore-engineered MOFs. TEM images of Ni-MOF-74 (c) and Ni-TPP (d).

S10). These NiMOF-74 analogues exhibit the same structure as that of the pore-expanded Mg-MOF-74.[19] The shift of the 2θ position of the Bragg peaks to the lower values while increasing the pore size of the MOFs indicates that the lattice parameters are increasing (Figure 2a). The cell volumes of 3323 $Å^3$ for Ni-MOF-74 increase to 9578 and 14 680 $Å^3$ for Ni-BPP and Ni-TPP, respectively (Figure S10), confirming that the longer chain aromatic linkers lead to a 2.9 and 4.4 times expansion of the framework. Each Ni^{2+} node has 6 coordination sites, 5 of which are occupied by oxygen from linkers. Under ambient conditions, the sixth site coordinates a water molecule, which can be removed by heat treatment (Figure S14). The nitrogen sorption isotherms for all samples exhibit type-I sorption (Figure S12a), but with an additional step in the relative pressure P/P_0 of 0.02 to 0.05 for Ni-BPP and 0.05 to 0.15 for Ni-TPP, indicating the difference in the pore size. As summarized in Figure 2 and Table S1, the pore apertures (11, 17, and 23 Å) and pore volume (0.49, 0.83, and 1.14 m^3/g) increase in the order Ni-MOF-74 < Ni-BPP < Ni-TPP.

The adsorption−desorption isotherms of water at 298 K are shown in Figure 3a. Ni-MOF-74 exhibits a type-I adsorption

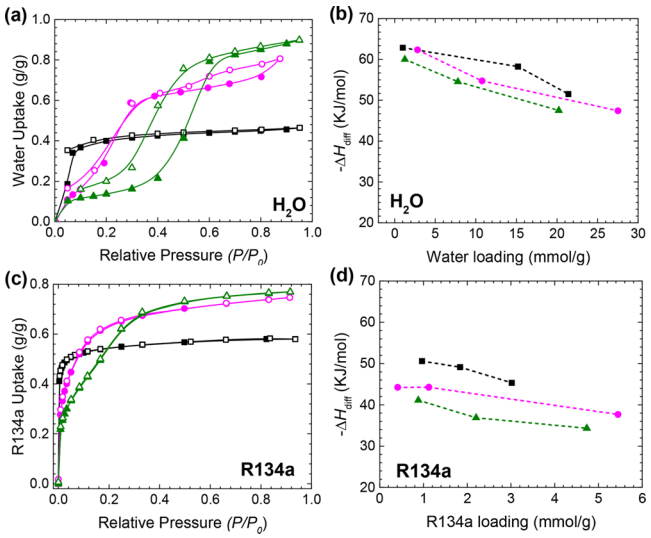

Figure 3. Adsorption (solid) and desorption (open) isotherms (a, c) and the differential heats (b, d) of H_2O and R134a adsorbed in MOFs. The P_0 for water and R134a at 298 K are 31.7 and 6078 mbar. The black, magenta, and green curves correspond to Ni-MOF-74, Ni-BPP, and Ni-TPP, respectively.

isotherm with a steep slope related to a large water uptake at low partial pressure (P/P_0 = 0 to 0.08), indicative of its high hydrophilicity. The total water uptake of 0.46 g g^{-1} is consistent with previous reports.[22] Ni-BPP displays a modified type-I-like isotherm. Fast water loading (0.11 g g^{-1}) occurs in the relative pressure range of 0 to 0.05. Then the main channel fills in two substeps. Ultimately, water uptake by Ni-BPP at high relative vapor pressures is extremely high (0.81 g g^{-1}). Further, Ni-TPP exhibits a type-IV isotherm with monolayer adsorbed water gives a steep slope at $P/P_0 < 0.05$. The huge amount of water adsorption at P/P_0 = 0.4 to 0.6 is beneficial for an adsorption cooling system because it indicates a large working capacity can be easily achieved, even for a narrow range of pressures. It is worth noting that 0.9 g g^{-1} water uptake in Ni-TPP is one of the highest water sorption capacities to date for currently

DOI: 10.1021/jacs.7b04872
J. Am. Chem. Soc. 2017, 139, 10601−10604

reported MOFs and only surpassed by the MIL-101 family (0.9−1.3 g g^{-1}).[23]

The R-134a isotherms for all three MOFs exhibit type-I character, and we observed a weak stepwise profile for the pore-expanded analogues (Figure 3c). Uptakes of R134a at extremely low partial pressure (P/P_0 = 0.02) are 0.48, 0.37, and 0.28 g g^{-1} for Ni-MOF-74, Ni-BPP, and Ni-TPP, respectively. This is consistent that the sorbate tends to fill the micropores in the low partial pressure region. In general, all three MOFs exhibit considerable amounts of R134a uptake at low partial pressures, indicating that MOFs with high density of open metal sites play an important role in sorbate−sorbent interactions. As the vapor pressure further increases, the loading of R134a is found to increase in the pore-expanded MOF-74 analogues. The saturation capacities are 0.58, 0.75, and 0.77 g g^{-1} for Ni-MOF-74, Ni-BPP, and Ni-TPP, respectively. Only a small increase in R134a uptake (0.02 gg^{-1}) is observed in Ni-TPP when compared to Ni-BPP. The higher uptake in Ni-BPP is attributed to a higher surface area that leads to more sorbate−sorbent interactions, whereas in Ni-TPP, though the surface area was slightly smaller, its total pore volume is higher due to the three-phenylene rings. This results in more adsorbate−adsorbent (C−F−M/C−H−π) interactions, respectively.

To further understand the adsorbate−adsorbent interactions, we measured the enthalpies of adsorption using a calorimetric method, a model-independent measure. The enthalpies of H_2O adsorption (Figure 3b) at low partial pressure or low water loading are −62.6, −62.1, and −60.0 kJ/mol, respectively, for the MOF-74 analogues. The large exothermic heat effect is consistent with IR results that suggest that H_2O is strongly bonded to the open Ni^{2+} site in the initial stage. But as the pore size increased, the enthalpies decrease significantly (up to ∼25%) as more H_2O is loaded. This may be due to the increasing distance between the open metal sites. In the case of R134a (Figure 3d), the enthalpies of adsorption are −50.6 (Ni-MOF-74), −44.2 (Ni-BPP), and −40.6 kJ/mol (Ni-TPP) at low loading, as expected with the sorption kinetics data (Figure 3c). The decrease in enthalpies with increased R134a loading was found to be small in all three MOFs (∼10% in value), attributed to R134a being a bigger molecule. Also, the favorable adsorbate−adsorbent interactions at higher loadings might have played a greater role. In general, for both H_2O and fluorocarbon, the heat of adsorption decreases as the pore size of the MOFs increases.

To understand the influence of pore environment on sorbate−MOF interaction on an atomistic level, *in situ* FTIR spectroscopy during water and R134a adsorption was employed. For H_2O adsorption, peaks <1500 cm^{-1} are mainly attributed to strong perturbations of the MOF's phonon modes (Figure S20). Thus, we only focus on O−H vibrational regions, i.e., 1500−1800 cm^{-1} and 3000−3800 cm^{-1}. Figure 4a shows the IR spectra of H_2O adsorption in Ni-BPP. The peaks at 3659 and 3568 cm^{-1} are assigned to the O−H interaction between adsorbed H_2O and open metal sites.[24] These peaks appear at very low partial pressures (10^{-5} mbar) and simultaneously grow until the vapor pressure reaches 0.1 mbar, consistent with the assumption that initially, water molecules are dissociatively adsorbed on the metal sites.[24] Peaks at 3221 and 3310 cm^{-1} are associated with the O−H stretch of hydrogen-bonded water.[25] The bands only appear when the vapor pressure reaches 0.1 mbar and grow rapidly as pressure increases. This is also consistent with the assumption that the second step of water

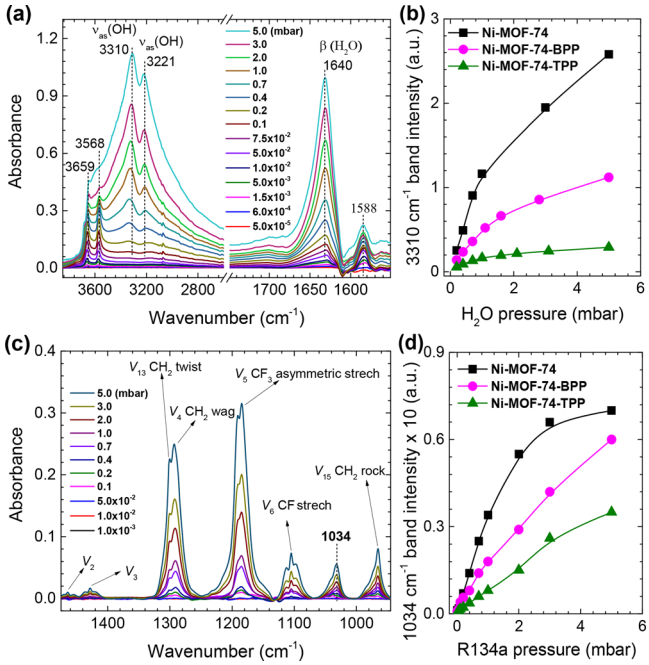

Figure 4. IR spectra of H_2O and R134a adsorbed in Ni-BPP under different vapor pressures (water, 0.000 05 to 5 mbar; R134a, 0.001 to 5 mbar) at 298 K (a and c). Regression of the height of IR bands at 3310 cm^{-1} for H_2O adsorption (b) and at 1034 cm^{-1} for Ni−F_3C (d) as pore size increases from Ni-MOF-74 to Ni-BPP and Ni-TPP.

loading involves filling the pores with hydrogen-bonded water, confirmed by the hydrogen-bonded β (H_2O) peak near 1640 cm^{-1}.[24] Similar spectra are observed from H_2O adsorbed in Ni-MOF-74 and Ni-TPP, indicating similar water adsorption mechanisms for the MOFs (Figures S21).

Vapor pressure evolution of the IR band intensities of hydrogen-bonded H_2O (3310 cm^{-1}) are shown in Figure 4b. For all three MOFs, the first appearance of bands corresponding to hydrogen-bonded H_2O occurs at the pressure of 0.1 mbar. These results demonstrate that 298 K, 0.1 mbar (P/P_0 = 0.003) might be the critical point for which a change in the mechanism of water loading occurs. This value does not change with pore size (despite the change in intensity). For the MOFs with identical Ni^{2+} nodes, smaller pores facilitate the H_2O to dissociatively adsorb on metal sites and also form hydrogen bonds. We have also performed *in situ* FTIR analysis of D_2O adsorption, which further verifies the findings from H_2O adsorption (Figure S22).

In situ FTIR analysis of R134a adsorption in Ni-BPP is shown in Figures 4c and S24. For R134a interacting with all three MOFs, we observe infrared spectra similar to gaseous species (compare Figures 4c, S23, and S24). One striking difference for the gaseous R134a infrared spectrum and those of the adsorbed R134a is a new band centered at ∼1034 cm^{-1} for all three MOFs. Moreover, the band intensity was found to increase as the pressure rises from 0.01 to 5 mbar (Figure 4d). It is worth noting that the rate of increase of the 1034 cm^{-1} band intensity with increase of R134a pressure decreases when going from Ni-MOF-74 to Ni-BPP to Ni-TPP. This matches well with the sorption kinetics observed in these MOFs (Figure S15) where a steep peak with 30% uptake in Ni-MOF-74 within 1 min, whereas taking at least 3 min to reach 21 and 18 wt % for Ni-BPP and Ni-TPP, respectively. The 1034 cm^{-1} band is hypothesized to correspond to the C−F stretching

DOI: 10.1021/jacs.7b04872
J. Am. Chem. Soc. 2017, 139, 10601−10604

frequency in R134a that bonds to open metal centers (Ni^{2+} nodes) in MOFs.

To validate this hypothesis, we performed three different experiments. First, we measured *in situ* IR of R134a adsorbed in the 2,5-dihydroxyterephthalic acid (DHTA), the organic linker of Ni-MOF-74; second, UiO-66 containing no open metal centers. In both cases, we did not observe this band (Figure S25). Lastly, another fluorocarbon, hexafluoroethane (CF_3−CF_3), was chosen given its close resemblance to R134a. As expected, the absorption band appeared, but with a slight upward shift to ∼1040 cm^{-1}. There is no IR peak in this region for the free hexafluoroethane. These experimental results suggest that the peak at 1034 cm^{-1} is assigned to a C−F stretch of the CF_3 moiety that is perturbed by the interaction of one of the fluorines with Ni^{2+} node. It is also worth noting that such high sensitivity of the 1034 cm^{-1} band at very low pressures (0.001 mbar) in Ni-MOF-74 opens a new area of refrigerant leak detection, a major problem in the adsorption cooling/refrigeration industry.

In summary, we have successfully synthesized a pore-engineered Ni-MOF-74 family and tested their performance toward water and fluorocarbon adsorption. Pore-expanded Ni-MOF-74 analogues show higher water and R134a uptake. The Ni-TPP gives 0.9 g g^{-1} water uptake, which we found to be one of the best water sorbing materials reported to date. *In situ* FTIR analysis further clarifies the adsorption mechanisms of water and R134a in MOFs. The findings suggest that pore engineering is an excellent strategy to enhance the loading of guest molecules in porous MOFs. This fluorocarbon/MOF combination has the potential to be one of the most promising working pairs for use in adsorption cooling applications.

■ ASSOCIATED CONTENT

Supporting Information

The Supporting Information is available free of charge on the ACS Publications website at DOI: 10.1021/jacs.7b04872.

Detailed experimental procedures, structure models, PXRD, SEM/TEM, TGA, kinetics measurement, calorimetric tests, R12 adsorption and additional IR data (PDF)

■ AUTHOR INFORMATION

Corresponding Author

*radhakishan.motkuri@pnnl.gov

ORCID

Jian Zheng: 0000-0003-2054-9482

Tamas Varga: 0000-0002-5492-866X

Radha Kishan Motkuri: 0000-0002-2079-4798

Notes

The authors declare no competing financial interest.

■ ACKNOWLEDGMENTS

The authors acknowledge U.S. Department of Energy (DOE), Energy Efficiency and Renewable Energy's Geothermal Technologies Office (GTO) for financial support. PNNL is operated by Battelle for the U.S. Department of Energy (DOE) under Contract DE-AC05-76RL01830.

■ REFERENCES

(1) Deng, J.; Wang, R. Z.; Han, G. Y. *Prog. Energy Combust. Sci.* **2011**, *37*, 172.

(2) U.S. Energy Information Administration. 2015 RECS Survey Data; https://www.eia.gov/consumption/residential/data/2015 (accessed February 27, 2017).

(3) Motkuri, R. K.; Annapureddy, H. V.; Vijaykumar, M.; Schaef, H. T.; Martin, P. F.; McGrail, B. P.; Dang, L. X.; Krishna, R.; Thallapally, P. K. *Nat. Commun.* **2014**, *5*, 4368.

(4) Mondloch, J. E.; Katz, M. J.; Planas, N.; Semrouni, D.; Gagliardi, L.; Hupp, J. T.; Farha, O. K. *Chem. Commun.* **2014**, *50*, 8944.

(5) Henninger, S. K.; Habib, H. A.; Janiak, C. *J. Am. Chem. Soc.* **2009**, *131*, 2776.

(6) Burtch, N. C.; Jasuja, H.; Walton, K. S. *Chem. Rev.* **2014**, *114*, 10575.

(7) Canivet, J.; Fateeva, A.; Guo, Y.; Coasne, B.; Farrusseng, D. *Chem. Soc. Rev.* **2014**, *43*, 5594.

(8) Furukawa, H.; Gandara, F.; Zhang, Y. B.; Jiang, J. C.; Queen, W. L.; Hudson, M. R.; Yaghi, O. M. *J. Am. Chem. Soc.* **2014**, *136*, 4369.

(9) Lin, R. B.; Li, T. Y.; Zhou, H. L.; He, C. T.; Zhang, J. P.; Chen, X. M. *Chem. Sci.* **2015**, *6*, 2516.

(10) Chen, T. H.; Popov, I.; Kaveevivitchai, W.; Chuang, Y. C.; Chen, Y. S.; Jacobson, A. J.; Miljanic, O. S. *Angew. Chem., Int. Ed.* **2015**, *54*, 13902.

(11) Eddaoudi, M.; Kim, J.; Rosi, N.; Vodak, D.; Wachter, J.; O'Keeffe, M.; Yaghi, O. M. *Science* **2002**, *295*, 469.

(12) Nijem, N.; Wu, H. H.; Canepa, P.; Marti, A.; Balkus, K. J.; Thonhauser, T.; Li, J.; Chabal, Y. J. *J. Am. Chem. Soc.* **2012**, *134*, 15201.

(13) Sun, Q.; Aguila, B.; Perman, J.; Earl, L. D.; Abney, C. W.; Cheng, Y. C.; Wei, H.; Nguyen, N.; Wojtas, L.; Ma, S. Q. *J. Am. Chem. Soc.* **2017**, *139*, 2786.

(14) Xiao, D. J.; Oktawiec, J.; Milner, P. J.; Long, J. R. *J. Am. Chem. Soc.* **2016**, *138*, 14371.

(15) Senkovska, I.; Barea, E.; Navarro, J. A. R.; Kaskel, S. *Microporous Mesoporous Mater.* **2012**, *156*, 115.

(16) Kim, H.; Yang, S.; Rao, S. R.; Narayanan, S.; Kapustin, E. A.; Furukawa, H.; Umans, A. S.; Yaghi, O. M.; Wang, E. N. *Science* **2017**, *356*, 430.

(17) Sun, L.; Campbell, M. G.; Dinca, M. *Angew. Chem., Int. Ed.* **2016**, *55*, 3566.

(18) Caskey, S. R.; Wong-Foy, A. G.; Matzger, A. J. *J. Am. Chem. Soc.* **2008**, *130*, 10870.

(19) Deng, H.; Grunder, S.; Cordova, K. E.; Valente, C.; Furukawa, H.; Hmadeh, M.; Gandara, F.; Whalley, A. C.; Liu, Z.; Asahina, S.; Kazumori, H.; O'Keeffe, M.; Terasaki, O.; Stoddart, J. F.; Yaghi, O. M. *Science* **2012**, *336*, 1018.

(20) Cho, H. S.; Deng, H. X.; Miyasaka, K.; Dong, Z. Y.; Cho, M.; Neimark, A. V.; Kang, J. K.; Yaghi, O. M.; Terasaki, O. *Nature* **2015**, *527*, 503.

(21) DeCoste, J. B.; Peterson, G. W.; Schindler, B. J.; Killops, K. L.; Browe, M. A.; Mahle, J. J. *J. Mater. Chem. A* **2013**, *1*, 11922.

(22) Liu, J.; Wang, Y.; Benin, A. I.; Jakubczak, P.; Willis, R. R.; LeVan, M. D. *Langmuir* **2010**, *26*, 14301.

(23) Henninger, S. K.; Jeremias, F.; Kummer, H.; Janiak, C. *Eur. J. Inorg. Chem.* **2012**, *2012*, 2625.

(24) Tan, K.; Zuluaga, S.; Gong, Q. H.; Canepa, P.; Wang, H.; Li, J.; Chabal, Y. J.; Thonhauser, T. *Chem. Mater.* **2014**, *26*, 6886.

(25) Nijem, N.; Canepa, P.; Kaipa, U.; Tan, K.; Roodenko, K.; Tekarli, S.; Halbert, J.; Oswald, I. W. H.; Arvapally, R. K.; Yang, C.; Thonhauser, T.; Omary, M. A.; Chabal, Y. J. *J. Am. Chem. Soc.* **2013**, *135*, 12615.

DOI: 10.1021/jacs.7b04872
J. Am. Chem. Soc. 2017, 139, 10601−10604